Article

Cell Reports

Common Regulatory Pathways Mediate Activity of MicroRNAs Inducing Cardiomyocyte Proliferation

Graphical Abstract

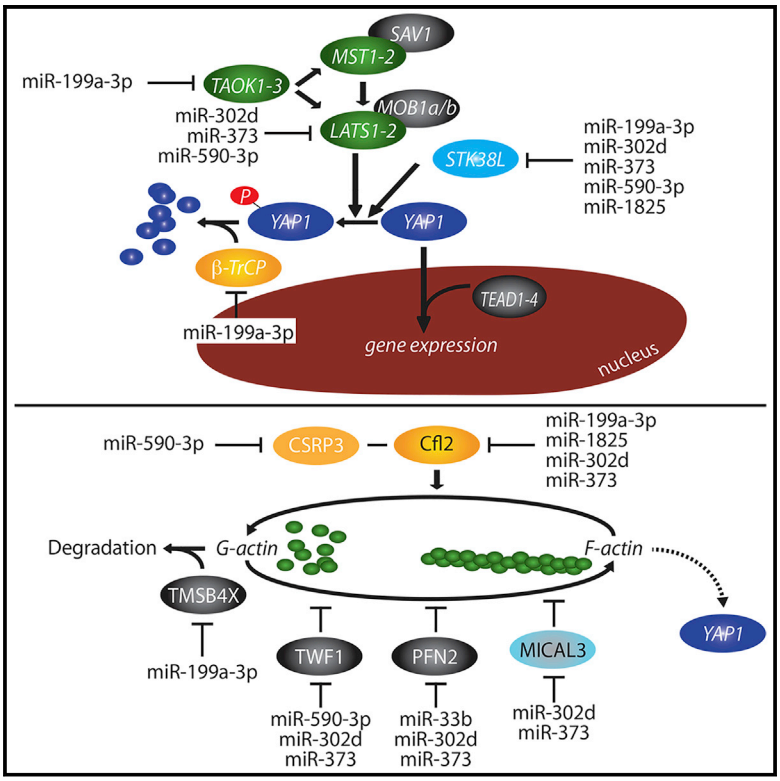

Highlights

- A few microRNAs can stimulate cardiac myocyte proliferation
- The most effective of these microRNAs activate YAP
- Several pro-proliferative microRNAs also inhibit actin depolymerization
- miR-199a-3p directly targets TAOK1, b-TrCP, and Cofilin2 to achieve its effects

Authors

Consuelo Torrini, Ryan John Cubero, Ellen Dirkx, ..., Matteo Marsili, Areejit Samal, Mauro Giacca

Correspondence

mauro.giacca@kcl.ac.uk

In Brief

Torrini et al. report that several microRNAs that induce cardiomyocyte proliferation act by stimulating activation of the transcriptional cofactor YAP, a master regulator of cell proliferation. Several microRNAs also act on the cardiomyocyte cytoskeleton by promoting actin polymerization. These microRNAs can be considered as potential treatments for cardiac regeneration.

Torrini et al., 2019, Cell Reports *27*, 2759–2771
May 28, 2019
https://doi.org/10.1016/j.celrep.2019.05.005

CellPress

Cell Reports
Article

Common Regulatory Pathways Mediate Activity of MicroRNAs Inducing Cardiomyocyte Proliferation

Consuelo Torrini,[1,8] Ryan John Cubero,[2,3,9] Ellen Dirkx,[1,10] Luca Braga,[1,4] Hashim Ali,[1,4] Giulia Prosdocimo,[1] Maria Ines Gutierrez,[1] Chiara Collesi,[1,5] Danilo Licastro,[6] Lorena Zentilin,[1] Miguel Mano,[1,11] Serena Zacchigna,[1,5] Michele Vendruscolo,[7] Matteo Marsili,[2] Areejit Samal,[2,12] and Mauro Giacca[1,4,5,13,*]

[1]Molecular Medicine Laboratory, International Centre for Genetic Engineering and Biotechnology (ICGEB), 34149 Trieste, Italy
[2]The Abdus Salam International Centre for Theoretical Physics, 34151 Trieste, Italy
[3]Scuola Internazionale Superiore di Studi Avanzati, 34136 Trieste, Italy
[4]School of Cardiovascular Medicine and Sciences, King's College London British Heart Foundation Centre, London SE5 9NU, UK
[5]Department of Medical, Surgical and Health Sciences, University of Trieste, 34127 Trieste, Italy
[6]CBM S.c.r.l., Area Science Park, Basovizza, 34149 Trieste, Italy
[7]Department of Chemistry, University of Cambridge, Lensfield Road, Cambridge CB2 1EW, UK
[8]Present address: Department of Pathology and Cell Biology, Columbia University Medical Center, New York, NY 10032, USA
[9]Present address: Centre for Neural Computation, Kavli Institute for Systems Neuroscience, Norwegian University of Science and Technology, 7030 Trondheim, Norway
[10]Present address: Department of Cardiology, CARIM School for Cardiovascular Diseases, Maastricht University, 6229 ER Maastricht, the Netherlands
[11]Present address: Functional Genomics and RNAi-Based Therapeutics Laboratory, Center for Neuroscience and Cell Biology, University of Coimbra, Coimbra, Portugal
[12]Present address: The Institute of Mathematical Sciences, Homi Bhabha National Institute, Chennai 600113, India
[13]Lead Contact
*Correspondence: mauro.giacca@kcl.ac.uk
https://doi.org/10.1016/j.celrep.2019.05.005

SUMMARY

Loss of functional cardiomyocytes is a major determinant of heart failure after myocardial infarction. Previous high throughput screening studies have identified a few microRNAs (miRNAs) that can induce cardiomyocyte proliferation and stimulate cardiac regeneration in mice. Here, we show that all of the most effective of these miRNAs activate nuclear localization of the master transcriptional cofactor Yes-associated protein (YAP) and induce expression of YAP-responsive genes. In particular, miR-199a-3p directly targets two mRNAs coding for proteins impinging on the Hippo pathway, the upstream YAP inhibitory kinase TAOK1, and the E3 ubiquitin ligase β-TrCP, which leads to YAP degradation. Several of the pro-proliferative miRNAs (including miR-199a-3p) also inhibit filamentous actin depolymerization by targeting Cofilin2, a process that by itself activates YAP nuclear translocation. Thus, activation of YAP and modulation of the actin cytoskeleton are major components of the pro-proliferative action of miR-199a-3p and other miRNAs that induce cardiomyocyte proliferation.

INTRODUCTION

Despite remarkable progresses made by surgical and medical therapies, the long-term survival of patients with heart disease remains poor. Cardiac injury, as a consequence of acute or chronic ischemia, hypertension, or inflammation, typically results in the irreversible loss of cardiomyocytes (CMs), which are incapable of clinically significant regeneration in the adult life. Scarring and fibrosis thus represent a general hallmark of cardiac repair and aging, with consequent progressive loss of cardiac function (for review, see Laflamme and Murry, 2011; Xin et al., 2013b; Zacchigna and Giacca, 2014).

Cardiac regeneration after damage, however, occurs in other species during the entire life (Bettencourt-Dias et al., 2003; Poss et al., 2002) and, in mammals, during the fetal and early post-natal periods (Porrello et al., 2011). Regeneration is sustained by the effective proliferation of already formed CMs, which only partially revert from their terminal differentiation state and re-enter the cell cycle, with no apparent involvement or stem or progenitor cell expansion (Eschenhagen et al., 2017). The reasons why, in mammals, this regenerative property is rapidly lost after birth are only partially understood and might be consequent to DNA damage caused by reactive oxygen species or to postnatal increase in mechanical load, both of which occur after birth (Canseco et al., 2015; Nakada et al., 2017). Whatever the mechanisms, the manipulation of the genetic programs that control CM proliferation by exogenous, therapeutic interventions might represent an innovative manner to achieve cardiac regeneration in adulthood.

In this context, increasing evidence indicates that CM proliferation in the embryonic and fetal life is under the control of the Hippo signal transduction pathway. In cardiac cells, the positive effector of this pathway is the transcriptional coactivator Yes-associated protein (YAP), which, in its de-phosphorylated form, localizes to nucleus and associates with the

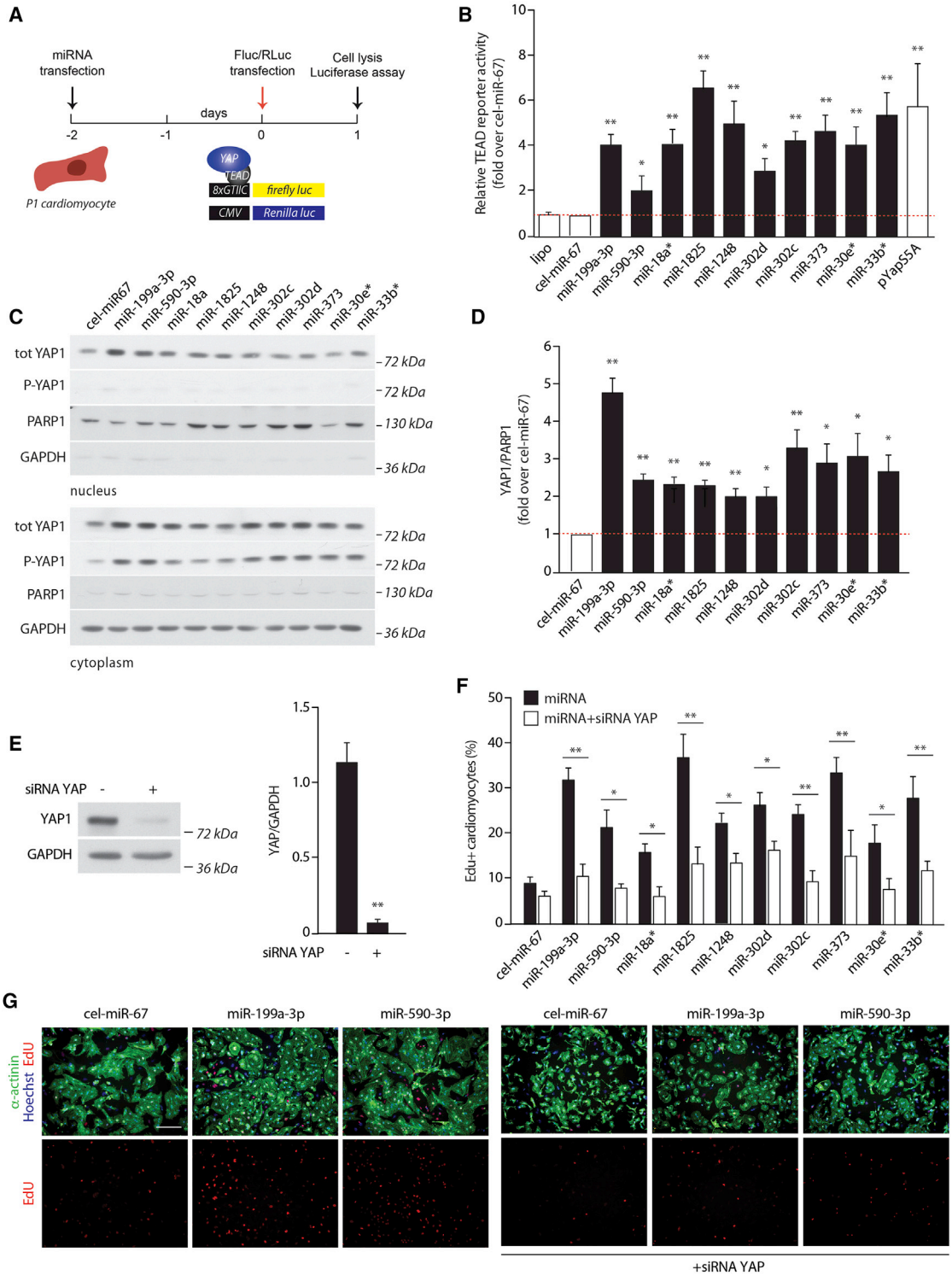

Figure 1. Activation of YAP Mediates Activity of miRNAs that Induce Cardiomyocyte Proliferation

(A) Experimental scheme to test activation of TEAD-dependent transcription.

(B) TEAD-luciferase reporter analysis of CMs transfected with the indicated miRNA mimics. Transfection efficiency was standardized over a constitutively expressed Renilla luciferase reporter. Transfection of a constitutively active YAP plasmid (pYAP5SA) served as a positive control. Data are mean ± SEM (n = 5 independent experiments); *p < 0.05, **p < 0.01; one-way ANOVA.

(legend continued on next page)

transcriptional enhanced associate domain (TEAD) 1–4 transcription factors to drive gene expression and stimulate cell proliferation. Deletion of floxed YAP alleles using Nkx2.5- or Tnnt2-drivers, which are expressed during early heart development, results in myocardial hypoplasia and early embryonic lethality (von Gise et al., 2012; Xin et al., 2011), while deletion of YAP at a later developmental stage leads to cardiac dilation and failure (Del Re et al., 2013; Xin et al., 2013a). On the contrary, transgenic overexpression of a constitutively active, nuclear YAP mutant causes CM hyper-proliferation (Xin et al., 2011, 2013a).

In resting CMs, YAP is maintained inactive in the cytoplasm by phosphorylation by a kinase cascade signaling. MST1/2 (Hippo in *Drosophila*, in which the pathway was originally discovered by genetic screens) (Pan, 2010; Saucedo and Edgar, 2007), in complex with SAV1, phosphorylates and activates LATS1/2, which associates with MOB1 and in turn phosphorylates and inactivates YAP. Genetic deletion of MST1, SAV1, and LATS determines cardiac hyperplasia (Heallen et al., 2011), while overexpression of MST1 (Yamamoto et al., 2003) or LATS2 (Matsui et al., 2008) leads to post-natal dilated cardiomyopathy, supporting the essential role of this pathway in the regulation of CM proliferation during embryonic and fetal development. Consistent with this notion, transgenic mice overexpressing activated YAP or lacking functional MST1 both repair myocardial injury through regeneration instead of fibrosis (Heallen et al., 2013; Xin et al., 2013a).

Work from several laboratories in the last few years has shown that most biological functions of CMs, including cell proliferation, are controlled by the microRNA (miRNA) network (Giacca and Zacchigna, 2015; van Rooij, 2011). In particular, a previous whole-genome, synthetic miRNA screening revealed several human miRNAs capable of inducing significant proliferation of neonatal rat and mouse CMs (Eulalio et al., 2012). Among these miRNAs were miR-199a-3p, miR-590-3p, miR-1248, miR-1825, and two large families of miRNAs, the miR-17/92 and the miR-302/367 cluster, which previous work has shown to be essentially involved in the regulation of embryonic cell proliferation (Barroso-del Jesus et al., 2009; Tiscornia and Izpisúa Belmonte, 2010). Transgenic mouse experiments indicate that both these miRNA families are involved in the regulation of cardiac cell proliferation during development, because their knockout leads to cardiac hypoplasia while, conversely, their overexpression expands the CM pool during embryogenesis (Chen et al., 2013; Tian et al., 2015). Of interest, at least two of the miRNAs that we identified, miR-199a-3p and miR-590-3p, were capable of inducing cardiac regeneration after myocardial infarction (MI), either when expressed using AAV vectors (Eulalio et al., 2012) or when delivered as naked miRNA mimics (Lesizza et al., 2017). Analogous findings were also achieved by systemic delivery of miR302b/c (Tian et al., 2015).

The identification of multiple miRNAs capable of inducing CM proliferation raises the obvious questions of whether they act through multiple or specific pathways, which are the individual mRNA targets that mediate their action, and to what extent they impact the molecular mechanisms known to regulate CM proliferation. The work described here aims to provide answers to these questions.

RESULTS

Activation of the YAP Transcriptional Coactivator Mediates the Function of miRNAs that Induce Cardiomyocyte Proliferation

We wanted to understand the mechanism of action of a series of human miRNAs that were previously shown to induce CM proliferation (Eulalio et al., 2012). These miRNAs included human miR-590-3p (the most effective in our original screening in rat cells), miR-199a-3p (the most effective in mouse cells), three members of the miR-302 family (miR-302d, miR-302c, and miR-373, known to be enriched in embryonic stem cells) (Barroso-del Jesus et al., 2009), miR-1825, miR-1248, miR-18a*, miR-33b*, and miR-30e*. Figure S1 reports the human sequences of these miRNAs and their levels of conservation in mouse, rat, and pig.

First, we assessed the possible involvement of the Hippo pathway in mediating the effect of these miRNAs. We started by analyzing the extent of TEAD activation by transfecting neonatal rat CMs with a TEAD-responsive, luciferase reporter plasmid together with each of these pro-proliferative miRNAs (scheme in Figure 1A). Transfection of constitutively activated YAP (YAP5SA) served as a positive control. We found that the TEAD reporter activity was significantly increased upon treatment with all the investigated miRNAs (Figure 1B). Next, we assessed the levels of cytoplasmic and nuclear (activated) YAP1 in miRNA-treated CMs. In all cases, cell treatment with the pro-proliferative miRNAs correlated with increased levels of non-phosphorylated YAP1 in the nucleus (Figures 1C and 1D for a representative western blot and quantification, respectively). Thus, miRNA transfection correlates with increased YAP activity in the cells.

We then wondered whether YAP activation was an essential requisite for the miRNAs to induce CM proliferation. To investigate this possibility, we knocked down YAP1 using a specific

(C) Induction of YAP nuclear translocation by treatment of CMs with pro-proliferative miRNAs. The western blots show the levels of nuclear and cytoplasmic YAP1 and phospho-YAP1 (P-YAP1) 72 h after transfection in a representative experiment. PARP1 and GAPDH were used for loading control of the nuclear and cytoplasmic fractions, respectively.

(D) Quantification of YAP nuclear translocation in CMs after miRNA mimics transfection. Results are shown as a ratio of YAP to nuclear PARP1. Data are mean ± SEM (n = 5 independent experiments); *p < 0.05, **p < 0.01; one-way ANOVA.

(E) Efficacy of YAP1 downregulation using a specific siRNA. On the left side, representative western blotting. On the right side, quantification of 3 independent experiments. Data are mean ± SEM; **p < 0.01; t test.

(F) Induction of CM proliferation by miRNA mimics is blunted by YAP knockdown. CMs were transfected with pro-proliferative miRNAs alone or in combination with an anti-YAP siRNA or the same amount of a non-targeting siRNA. The graph shows the percentage of sarcomeric α-actinin-positive cells that have incorporated EdU in a 72 h period. Data are mean ± SEM (n = 4 independent experiments); *p < 0.05, **p < 0.01; one-way ANOVA.

(G) Representative images of CMs treated with the indicated miRNAs with or out without a siRNA against YAP. Scale bar, 100 μm.

small interfering RNA (siRNA) (knockdown >85%; Figure 1E) and simultaneously treated CMs with the 10 miRNAs under investigation, followed by analysis of 5-ethynyl-2′-deoxyuridine (EdU) incorporation as a surrogate marker for cell proliferation. We found that, in all cases, YAP knockdown prevented the pro-proliferative effect of all the investigated miRNAs (Figure 1F). Representative images of proliferating CM cultures in response to treatment with miR-199a-3p and miR-590-3p, and inhibition of their effect upon YAP downregulation are shown in Figure 1G. Our previous published results (Eulalio et al., 2012) and unpublished data indicate that all 10 of the analyzed miRNAs, in addition to inducing DNA synthesis as measured by EdU incorporation, also stimulate cell passage through G2/M (H3-Ser10 phosphorylation; cf. also Figure 5) and karyokinesis (Aurora B localization in midbodies).

From these experiments, we conclude that increase in YAP nuclear activity is an essential requisite to mediate induction of CM proliferation by the 10 investigated miRNAs.

Identification of mRNA Targets Mediating miRNA-Induced YAP Activation

We next investigated the mechanism by which the 10 proliferative miRNAs lead to YAP activation. First, we generated a catalog of the genes known to participate, either directly or indirectly, in the regulation of YAP transactivation (203 genes); for each of these genes we annotated the bioinformatics prediction of miRNA targeting according to the TargetScan software (Table S1). Because of the large number of cataloged genes in the Hippo pathway, we performed a total RNA sequencing (RNA-seq) analysis to narrow down the list of candidates to a smaller set of genes. To this effect, we transfected neonatal rat CMs with 6 of the investigated miRNAs (miR-590-3p, miR-199a-3p, miR-1825, miR-302d, miR-373, and miR-33b*) and determined the resulting transcriptional profile (Figure S2A). Cluster analyses of these RNA profiles indicated that miR-302d and miR-373-3p had similar effects in terms of target gene regulation (Figure S2B), as expected from their common seed sequence. The genes that were either downregulated (n = 96 in total) or upregulated (n = 156) by all six miRNAs are shown in Figure S2C. The effects of these miRNAs on the genes involved in the Hippo pathway are reported in Table S1 and summarized in Figure S2D, in which the levels of each of the differentially regulated transcripts in the Hippo pathway is shown along its fold difference over control (green, downregulated genes; red, upregulated genes). While this RNA-seq analysis, being performed on a single replicate, did not possess statistical significance of the differentially expressed genes under each miRNA transfection, it did, however allow indication of common genes and pathways shared by all miRNAs. The concordant information between RNA-seq and target prediction is summarized in the cartoon shown in Figure 2A. Based on this information, we then focused our attention on the mechanism of action of the individual miRNAs.

Previous work has already shown that miR302-367 downregulates MST1, LATS2, and MOB1b in the Hippo pathway (Tian et al., 2015). As far as miR-199a-3p is concerned, CM treatment with this miRNA resulted in the downregulation both the TAO kinase1 (TAOK1) and the E3 ubiquitin-ligase β-transducing repeat containing protein (β-TrCP) (Figure S2D). TAOK1/3 was reported to phosphorylate and activate MST1/2 (Boggiano et al., 2011), as well as to act as direct kinases for LATS1/2 (Plouffe et al., 2016; Poon et al., 2011); β-TrCP, instead, catalyzes phosphorylated YAP ubiquitination, ultimately leading to its degradation (Zhao et al., 2010; cartoon in Figure 2A). We experimentally verified that CM treatment with miR-199a effectively downregulated the mRNAs for these two proteins (Figure 2B). In addition, we noticed that the STK38L kinase was a predicted target for 5 of the investigated miRNAs and that its levels were downregulated in all 6 RNA-seq profiles. Thus, we experimentally verified that the STK38L mRNA was reduced upon CM treatment with the six tested miRNAs (including miR-33b*, which was not predicted bioinformatically), with the exception of miR-590-3p (Figure 2C). Consistent with the information that miR-199a-3p downregulates the mRNAs coding for TAOK1, β-TrCP, and STK38L, we also found that the levels of the respective proteins were reduced in CMs treated with this miRNA (representative blot and quantification in Figures 2D and 2E, respectively).

Next, we assessed whether TAOK1, β-TrCP, and STK38L are direct targets of the investigated miRNAs. For this purpose, we cloned the 3′UTRs of the three genes downstream of the Renilla luciferase mRNA and transfected these plasmids into HeLa cells treated with the 10 pro-proliferative miRNAs. Simultaneous transfection of a plasmid encoding for firefly luciferase served as a transfection control, while the empty cloning vector (psiCheck2.1) was used for normalization (scheme in Figure 2F).

Analysis of luciferase activity after 48 h revealed that both TAOK1 and β-TrCP, but none of the other investigated miRNAs, were direct targets of miR-199a-3p (Figures 2G and 2H, respectively, for the results with miR-199a only, and Figures S3A and S3D for results will all the 10 pro-proliferative miRNAs), while none of the miRNAs targeted directly the 3′ UTR of STK38L (Figure 3I for the 6 miRNAs that downregulate STK38L mRNA and Figure S3G for all 10 miRNAs). Sequence analysis of the TAOK1 and β-TrCP 3′ UTRs revealed the presence of potential target sites for miR-199a-3p (Figures S3B and S3E, respectively). Mutation of these sites abrogated the downregulation effect for both genes, thus supporting the specificity of the miRNA-target mRNA interaction (Figures S3C and S3F).

Next, we investigated whether the downregulation of TAOK1, β-TrCP, or STK38L exerts a direct role in the regulation of CM proliferation. First, we generated siRNAs targeting each of the three genes; these siRNAs downregulated expression of the respective proteins, >90% in the case of TAOK1, >70% in the case of β-TrCP, and >50% in the case of STK38L, compared to control (representative blots and quantification in Figures 2J and 2K, respectively). Then we transfected these siRNAs in CMs and tested their proliferation. We found that the siRNAs against TAOK1 and β-TrCP stimulated CM EdU incorporation; their effect was suppressed by the simultaneous downregulation of YAP by RNAi (Figure 2L). In contrast, the individual siRNA against STK38L was ineffective. Figure S4 displays some representative images of CMs treated with siRNAs against TAOK1 and β-TrCP, with or without the siRNA against YAP. Consistent with these findings, we also found that the downregulation of TAOK1 and β-TrCP activated expression, in CMs, of the TEAD-responsive promoter (Figure 2M).

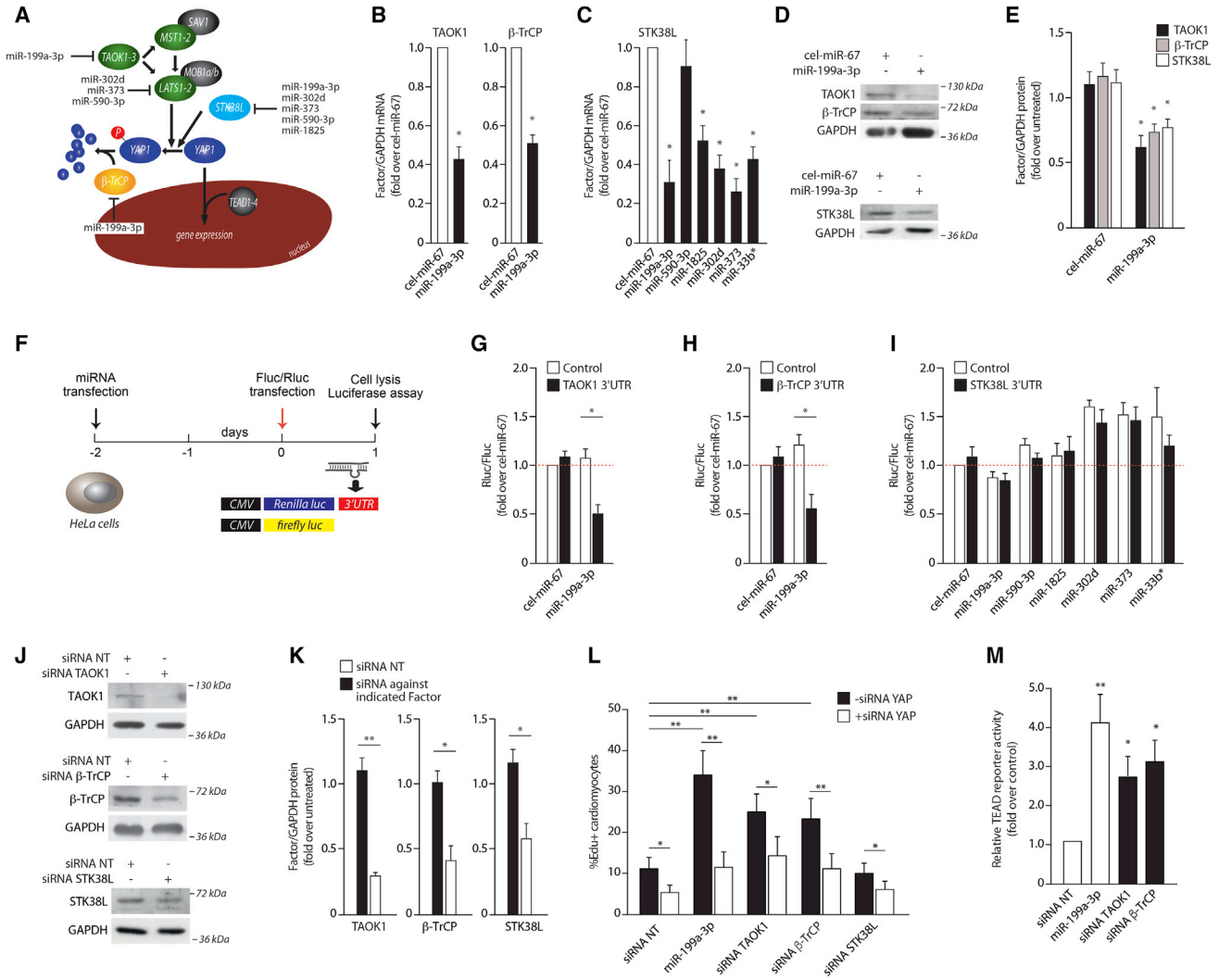

Figure 2. Mechanism for YAP Activation by miR-199a-3p and Other miRNAs

(A) Schematic representation of the Hippo pathway with the indication of the predicted target proteins according TargetScan software predictions.

(B) Real-time RT-PCR quantification of TAOK1 and β-TrCP mRNAs in CMs treated with miR-199a-3p mimic. Data are mean ± SEM of 3 independent experiments; *p < 0.05; t test.

(C) Real-time RT-PCR quantification of STK38L mRNA levels in CMs treated with the indicated miRNA mimics. Data are mean ± SEM of 3 independent experiments; *p < 0.05; one-way ANOVA.

(D and E) Representative western blots (D) and quantification (E) showing downregulation of TAOK1, β-TrCP and STK38L proteins in cells treated with miR-199a-3p mimic. Data are mean ± SEM of 3 independent experiments; *p < 0.05; t test.

(F) Experimental flow chart of 3′ UTR luciferase assays. Fluc and Rluc: firefly and Renilla luciferase genes, respectively.

(G and H) TAOK1 (G) and β-TrCP (H) are direct targets of miR-199a-3p. Results of 3′ UTR luciferase assays with miR-199a-3p. Renilla luciferase (Rluc) values were normalized over firefly (Fluc) values to standardize for transfection efficiency. Control refers to transfection of a Renilla luciferase gene with no 3′ UTR. Data are mean ± SEM (n = 3 independent experiments); *p < 0.05; t test.

(I) Results of 3′ UTR assays for STK38L in cells transfected with the indicated miRNA mimics.

(J and K) Representative western blots (J) and quantification (K) showing downregulation of TAOK, β-TrCP, and STK38L in CMs transfected with the respective siRNAs.

(L) Downregulation of TAOK1 and β-TrCP stimulates CM proliferation in a YAP-dependent manner. The graph shows the percentage of sarcomeric α-actinin-positive cells that have incorporated EdU in a 72 h period after treatment with specific siRNAs alone or in combination with an anti-YAP siRNA. Data are mean ± SEM (n = 4 independent experiments); *p < 0.05, **p < 0.01; one-way ANOVA.

(M) Downregulation of TAOK1 and β-TrCP stimulate transcriptional TEAD activity. CMs were transfected with siRNAs against TAOK1 or β-TrCP in combination with a TEAD-firefly luciferase reporter. The results were normalized to those of a constitutively expressed Renilla luciferase construct. Data are mean ± SEM over a non-targeting (NT) siRNA (n = 5 independent experiments); *p < 0.05; one-way ANOVA.

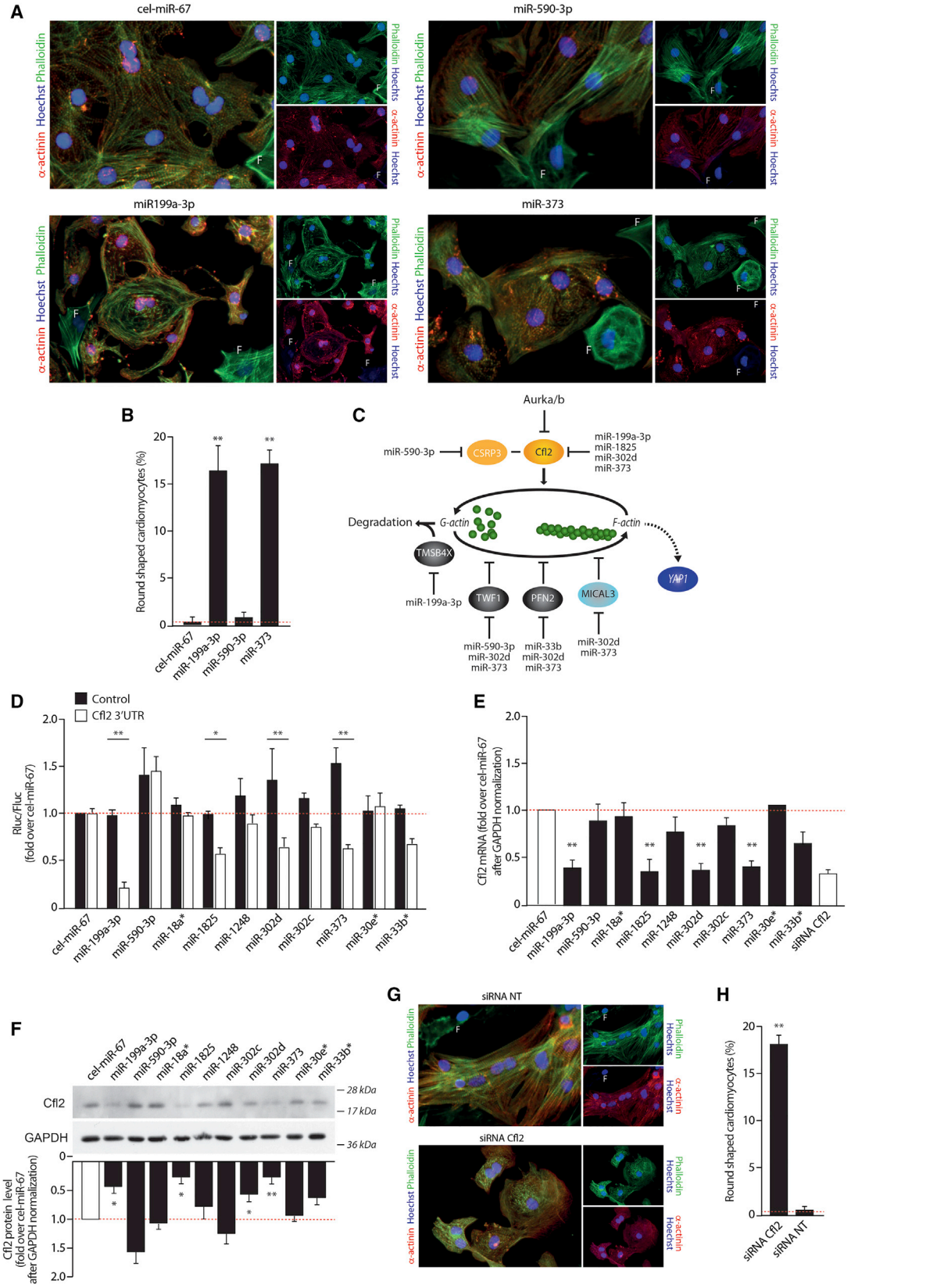

(legend on next page)

Taken together, these results reveal that the mechanism by which miR-199a-3p induces CM proliferation involves the direct targeting of two proteins, TAOK1 and β-TrCP, which individually participate in the regulation of YAP activity and the control of CM proliferation.

Modulation of the Actin Cytoskeleton by Cofilin-2 Regulates Cardiomyocyte Proliferation

While performing the above described experiments, we reproducibly noticed that CMs treated with some of the pro-proliferative miRNAs (most notably, miR-199a-3p and miR-373) induced a remarkable modification of cell shape. We thus wanted to examine the actin cytoskeleton using fluorescein-tagged phalloidin to visualize F-actin. In control cells treated with the *C. elegans* miR-67, actin was organized regularly in long threads throughout the cytoplasm, overlapping with those of the CM-specific, sarcomeric α-actinin (Figure 4A). In contrast, cells treated with miR-199a-3p and miR-373 were round-shaped, with actin fibers assembled in round bundles close to the cytoplasm periphery; these bundles of cortical actin were particularly evident in α-actinin-negative cells (fibroblasts). CMs treated with the two miRNAs also showed reduced organization of the sarcomere. No effect was detected in cultures treated with miR-590-3p. Figure 4B reports quantification of the number of round-shaped CMs upon miRNA treatment.

To follow up on this observation, we generated a catalog of 79 genes known to participate in, or regulate, formation of the microfilament cytoskeleton (Table S2). For each of these genes, we annotated the predicted targeting of each of the investigated miRNAs, and the extent of downregulation observed after CM treatment with each miRNA. The genes that were differentially regulated are shown in Figure S2D. These included various members of the 6 regulatory families coding for factors that normally prevent unwanted actin polymerization by directly interacting with G-actin, including Cofilin2 (Cfl2), Twinfilin1 and Twinfilin2 (Twf1 and Twf2), Thymosin β4 (Tmsb4x), and Profilin2 (Pfn2) (Xue and Robinson, 2013). Additionally downregulated proteins were Csrp3, Mical3, and Aurora A kinase (Aurka), all of which are directly or indirectly involved in the regulation of actin polymerization (Frémont et al., 2017; Papalouka et al., 2009; Ritchey and Chakrabarti, 2014). Figure 3C shows that several of these proteins were also predicted direct targets of the miRNAs by computational algorithms.

We focused our attention on the Cofilin2 mRNA, which was downregulated by all the investigated miRNAs, with the exception of miR-590-3p and was the predicted target of 4 of these miRNAs (miR-199a-3p, miR-1825, miR-302d, and miR-373). Indeed, we found that all 4 of these miRNAs targeted the Cofilin2 3′ UTR in UTR-luciferase assays (Figure 3D).

Quantification of mRNA levels in miRNA-treated CMs confirmed significant downregulation of the Cofilin2 mRNA in cells treated with these 4 miRNAs, in addition to CMs also treated with miR-33b* (Figure 3E). Downregulation of Cofilin2 by the last miRNA is likely an indirect effect or an effect exerted through binding of the miRNAs to portions of the Cofilin2 mRNA outside the 3′ UTR. Analysis of Cofilin2 protein levels in miRNA-treated CMs provided consistent results showing downregulation of this factor after treatment with miR-199a-3p, miR-1825, miR-302d, and miR-373 (Figure 3F). Sequence analysis of the Cofilin2 mRNA 3′ UTRs revealed the presence of a potential target site for miR-199a-3p. Mutation of this site abrogated the downregulation effect for this miRNA, thus supporting specificity (Figures S3H and S3I).

Finally, we observed that a similarly rounded shape and spatial arrangement of F-actin was also detected in cells transfected with the anti-Cofilin2 siRNA (representative images and quantification in Figures 3G and 3H, respectively).

Collectively, these results indicate that proteins regulating the actin cytoskeleton dynamics and, in particular, the inhibitor of F-actin polymerization Cofilin2, are frequently targeted, either directly or indirectly, by miRNAs that induce CM proliferation.

Remodeling of the Actin Cytoskeleton in Proliferating Cardiac Myocytes

Cofilin2 regulates the actin cytoskeleton by promoting conversion of polymerized F-actin back into its monomeric, G-actin form. We thus assessed the ratio between G- and F-actin in CMs treated with a few of the pro-proliferative miRNAs or with an siRNA against Cofilin2; this siRNA downregulated the levels of its target protein by >60% in CMs as well as upregulated the levels of F-actin, as shown by western blotting (Figure 4A).

The G/F ratio resulted decreased for CMs treated with all the tested miRNAs; this result reached statistical significance

Figure 3. Treatment of CMs with miRNAs Downregulates Cofilin2 and Induces Remodeling of the Actin Cytoskeleton

(A) Immunofluorescence pictures showing remodeling of the actin cytoskeleton upon miRNA treatment. F-actin is visualized using fluorescent phalloidin (green), CMs with an anti-α -actinin antibody (red), nuclei with Hoechst (blue). F indicates fibroblasts (α-actinin-negative cells).

(B) Percentage of CMs with a rounded shape (as in the representative images in A) after treatment of CMs with the indicated miRNAs. Data are from the analysis of over 400 CMs from four different experiments; shown are mean ± SEM; **p < 0.01; one-way ANOVA.

(C) Simplified view of proteins involved in actin cytoskeleton remodeling which are predicted to be targeted by the indicated pro-proliferative miRNAs.

(D) Results of 3′ UTR assays to evaluate direct targeting of Cofilin2 (Cfl2) by the investigated miRNAs. Experiments were performed as in Figure 2F. Data are mean ± SEM (n = 3 independent experiments); *p < 0.05; **p < 0.01; one-way ANOVA.

(E) Results of real-time RT-PCR quantification of the Cofilin2 mRNA in CMs treated with the indicated miRNA mimics. An siRNA against Cofilin2 (siCfl2) was used as a positive control. Data are mean ± SEM (n = 3 independent experiments); *p < 0.05; **p < 0.01; one-way ANOVA.

(F) Effect of miRNAs on Cofilin2 protein levels in CMs. Strip in the upper part: representative western blot showing downregulation of Cofilin2 in CMs transfected with the indicated miRNA mimics. Graph in the lower part: quantification of the levels of Cofilin2. Data are mean ± SEM (n = 3 independent experiments); *p < 0.05; **p < 0.01; one-way ANOVA. The dotted, red line shows the levels Cofilin2 in CMs treated with the control cel-miR-67 miRNA.

(G) Same as in (A) in CMs treated with an anti-Cofilin2 siRNA or with a non-targeting (NT) siRNA control.

(H) Percentage of CMs with a rounded shape (as in the representative images in G) after treatment of CMs with the Cofilin2 siRNA. Data are from the analysis of over 400 CMs from four different experiments; shown are mean ± SEM; **p < 0.01; t test.

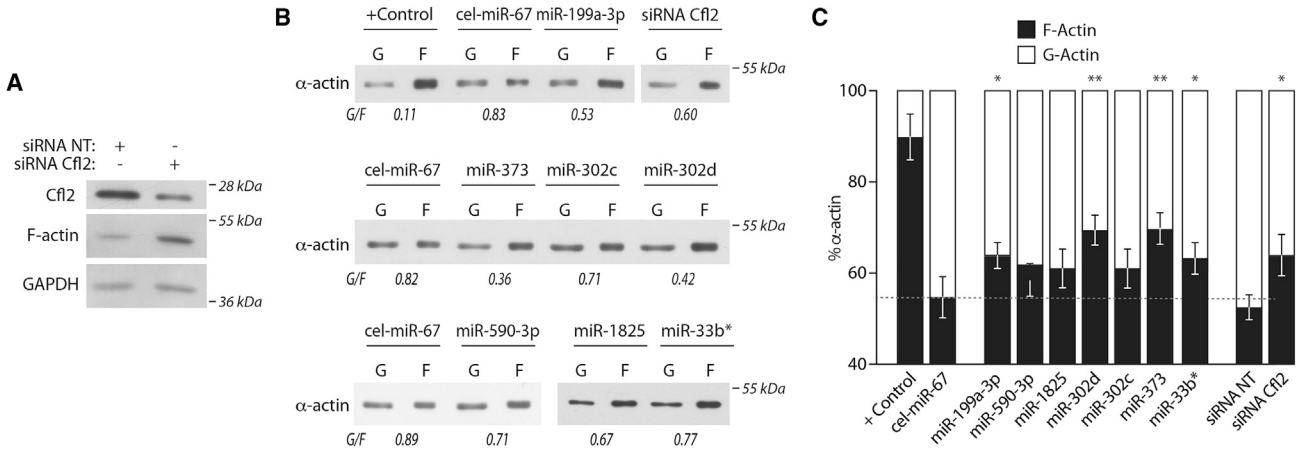

Figure 4. Treatment of CMs with miRNAs Induces Remodeling of the Actin Cytoskeleton

(A) Representative western blot showing that downregulation of Cofilin2 increases the levels of filamentous (F)-actin. siRNA NT, non-targeting siRNA control.

(B) Quantification of the G-actin/F-actin ratio in CMs treated with the indicated pro-proliferative miRNAs or with anti-Cofilin2 siRNA. The pictures show representative western blots, using an anti-α-actin antibody, of supernatants (containing G-actin) and pellets (F-actin) obtained by ultracentrifugation of lysates from the treated CMs. The G/F ratio is shown at the bottom of each band pair. The positive (+) control was provided by the kit manufacturer.

(C) Quantification of the G/F actin ratio, expressed in percentage, obtained as in (B). Data are mean ± SEM (n = 3 independent experiments); *p < 0.05; **p < 0.01; one-way ANOVA. The dotted, red line shows the G/F ratio in CMs treated with the control cel-miR-67 miRNA.

for miR-199a-3p, miR-373, miR-302d, and miR-33b* when compared to the *C. elegans* miRNA control. The G/F ratio was also decreased in cells treated with the anti-Cofilin2 siRNA (Figures 4B for representative blots and 4C for quantification).

Progression of the cell cycle toward G2 and mitosis was assessed in cells treated with miR-199a-3p, miR-590-3p, miR-373, or the anti-Cofilin2 siRNA by visualizing phosphohistone H3. As shown in the representative pictures in Figure 5A for the miRNAs, Figure 5B for the siRNA, and quantified in Figure 5C, all treatments induced 5%–9% of the cells to travel through the G2/M phase. Mitotic CMs showed disruption of the sarcomeric architecture, as concluded from the diffused staining with α-actinin shown in Figure 5D. Alpha-actinin-positive CMs in different phases of mitosis are shown in Figure 5E.

Downregulation of Cofilin2 Activates Cardiomyocyte Proliferation through YAP Activation

We asked whether activation of CM proliferation upon downregulation of Cofilin2 and actin cytoskeleton rearrangement might directly involve activation of YAP. Supporting this possibility, we found that in CMs, downregulation of Cofilin2 by RNAi determined transcriptional activation of the TEAD-dependent, YAP-responsive promoter (Figure 6A). Simultaneous transfection of CMs with an siRNA against YAP abrogated the pro-proliferative effect exerted by Cofilin2 downregulation, similar to its inhibitory effect on miR-199a-3p (Figure 6B; representative picture showing decreased number of cells incorporating EdU in Figure 6C). Finally, CM treatment with the anti-Cofilin2 siRNA showed marked activation of the mRNA levels of two well-established YAP-responsive genes, CTGF and CyR61 (Zhao et al., 2008; Figure 6D).

The above results are suggestive of a correlation between the extent of actin polymerization (that is increased by Cofilin2 inhibition) and the activation of YAP. To further explore this link, we inversely inhibited actin polymerization using cytochalasin D and then studied the levels of nuclear and cytoplasmic YAP. We found that CMs treated with this drug (that, as expected, also completely blocked EdU incorporation; data not shown), reduced the levels of nuclear YAP in a time-dependent manner, while increasing the amounts of the cytoplasmic, phosphorylated protein (representative western blots in Figure 6E and quantification in 6F). This effect resulted in marked suppression of the levels of the CTFG and CyR61 gene mRNAs (Figure 6G). On the contrary, CM treatment with the actin cytoskeleton stabilizing drug jasplakinolide (Wang et al., 2014a), when used at concentrations that were not toxic to the cells, significantly increased the levels of nuclear YAP1 (Figure S5).

Together, these results are consistent with the conclusion that, in CMs, the extent of actin polymerization regulates YAP nuclear activity and, as a consequence, controls the levels of cell proliferation.

Finally, we observed that nuclear translocation of YAP and activation of YAP-reporter genes was specific for miR-199a and cell treatment with the pro-hypertrophic drug phenylephrine, consistent with published results (Del Re et al., 2013; Wang et al., 2014b), while it did not occur upon CM treatment with a combination of FGF1 and a p38 inhibitor, a stimulus previously reported to also induce CM proliferation (Engel et al., 2005; Figure S6). These results confirmed specificity of the observed effects relating miRNA treatment with YAP activation.

DISCUSSION

In this work, we have described the mechanisms of action of a series of miRNAs that were recently shown to induce CM proliferation and are thus of interest for potential applications aimed at stimulating cardiac regeneration. In essence, the information that we obtained indicates that all these miRNAs converge in

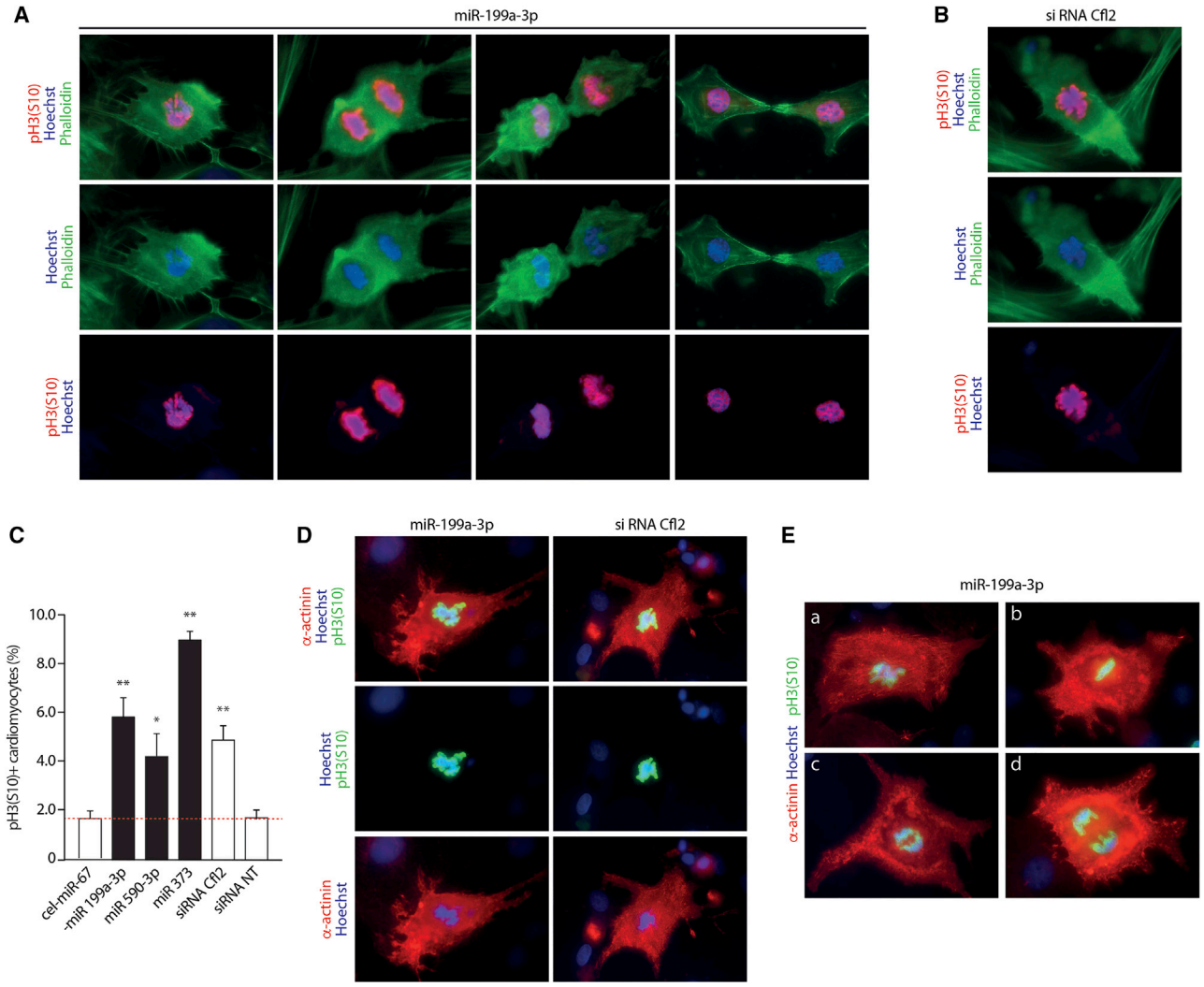

Figure 5. Disruption of the Sarcomeric Architecture in Mitotic Cardiomyocytes Treated with miR-199a-3p and Cofilin2 siRNA

(A and B) Representative pictures showing G2/M cells upon treatment with miR-199a-3p (A) or anti-Cofilin2 siRNA (B), showing nuclear positivity for phospho-histone H3 (pH3(S10), red) and diffused cytoplasmatic staining for α-actin (green). Nuclei are counterstained with Hoechst 33342 (blue).

(C) Percentage of pH3(S10)$^+$, α-actinin$^+$ cells (CMs) after treatment with the indicated miRNAs or Cofilin2 siRNA. Cel-miR-67 and a non-targeting (NT) siRNA served as negative controls for miRNA and siRNA experiments respectively. Data are from the analysis of over 400 CMs from four different experiments; shown are mean ± SEM; $^{**}p < 0.01$, $^{*}p < 0.05$; one-way ANOVA.

(D) Representative pictures of G2/M CMs (defined as in C), showing nuclear positivity for phospho-histone H3 (pH3(S10), red) and disruption of the sarcomeric architecture, as concluded from diffused staining of α-actinin (red). Nuclei are counterstained with Hoechst 33342 (blue).

(E) Mitotic CMs in subsequent phases of mitosis (from A to D). Staining as in (D).

the activation of nuclear translocation of the YAP transcriptional coactivator. This event is, however, achieved through the modulation of the levels of different effector genes, among which the regulation of actin cytoskeleton dynamics plays an essential role.

The proliferative miRNAs act through different pathways to achieve convergent YAP activation. Among the factors that are downregulated either directly or indirectly are one or more of the cellular kinases known to inactivate YAP, in particular TAOK1, LATS1/2, and STK38L. Our results show that miR-199a directly targets the 3′ UTR of TAOK1; previous work indicated that the miR-302/367 cluster (of which we analyzed miR-302c and miR-302d) downregulates the levels of MST1 and MOB1b, in addition to those of LATS2 (Tian et al., 2015). The levels of STK38L instead resulted downregulated upon CM treatment with 5 different miRNAs, but in no case could we detect direct targeting of the factor mRNA 3′ UTRs, indicating that either the effect is indirect, or it is exerted through binding of the miRNAs to different regions of the kinase mRNA. Convergence of CM pro-proliferative miRNAs onto the Hippo pathway was also recently shown by the Mercola laboratory after high throughput screening for miRNAs stimulating human iPS cell-derived CM proliferation (Diez-Cuñado et al., 2018).

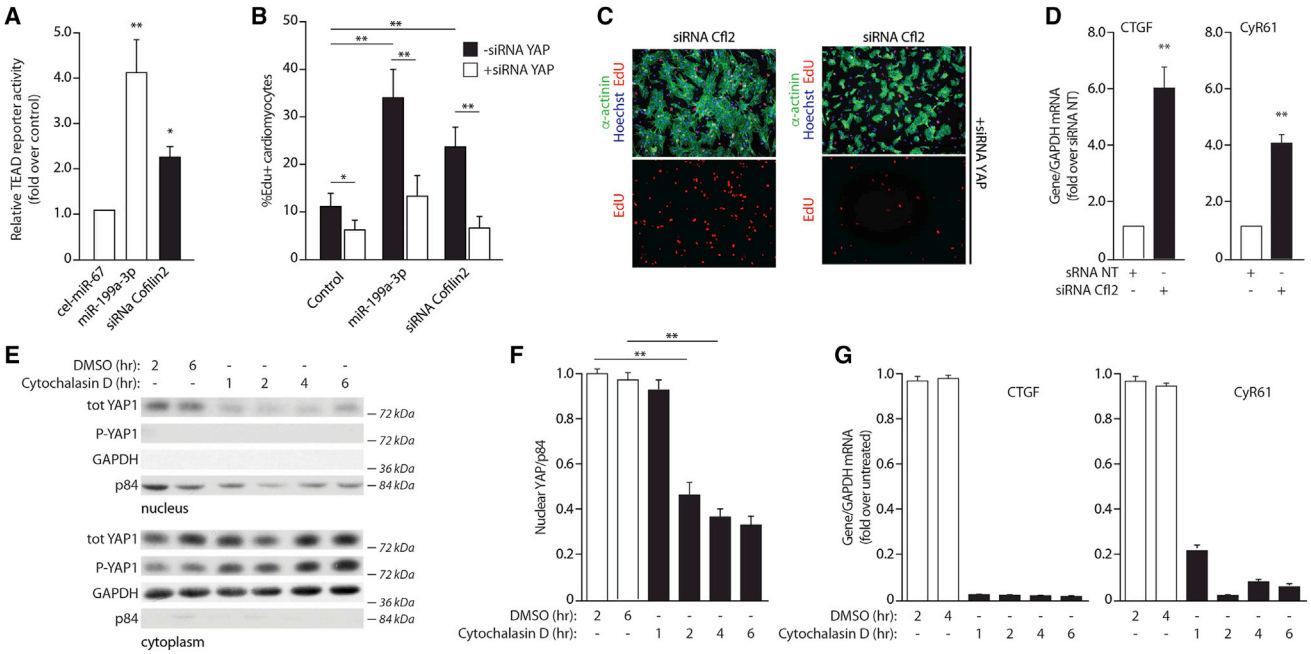

Figure 6. Perturbation of the Actin Cytoskeleton Activates YAP Nuclear Translocation and Activity

(A) Downregulation of Cofilin2 activates TEAD reporter activity. The graph reports the results of TEAD-firefly luciferase reporter analysis of CMs transfected with miR-199a-3p and Cofilin2 siRNA. Experiments were performed as in Figure 1A. Transfection efficiency was standardized over a constitutively expressed Renilla luciferase reporter. Data are mean ± SEM (n = 4 independent experiments); *p < 0.05, **p < 0.01; one-way ANOVA.

(B) Downregulation of Cofilin2 activates CM replication in a YAP-dependent manner. The graph shows the percentage of α-actinin-positive cells that have incorporated EdU in a 72 h period after treatment with anti-Cofilin2 siRNA or miR-199a-3p mimic alone or in combination with an anti-YAP siRNA. Data are mean ± SEM (n = 4 independent experiments); *p < 0.05, **p < 0.01; one-way ANOVA.

(C) Representative pictures showing CMs incorporating EdU after treatment with an anti-Cofilin2 siRNA as in (B) in the absence or presence of an anti-YAP siRNA.

(D) Real-time RT-PCR analysis of the levels of the two TEAD responsive genes CTFG and CyR61 in CMs transfected with anti-Cofilin2 siRNA. Data are mean ± SEM (n = 4 independent experiments); **p < 0.01; t test.

(E) Treatment of CMs with cytochalasin D blocks nuclear translocation of YAP. Representative blots showing the levels of nuclear and cytoplasmic YAP1 and phospho-YAP1 (P-YAP1) in CMs treated with cytochalasin D for the indicated time points. GAPDH and p84 were used for loading controls of cytoplasmic and nuclear fractions, respectively.

(F) Quantification of YAP nuclear translocation in CMs treated with cytochalasin D. Data are mean ± SEM (n = 3 independent experiments); **p < 0.01; one-way ANOVA.

(G) Treatment with cytochalasin D blocks transcription of YAP-responsive genes. The graph shows the levels of the CTFG and CyR61 mRNAs, measured by real-time RT-PCR, in CMs treated with cytochalasin D for the indicated time points. Data are mean ± SEM (n = 3 independent experiments). All times showed statistical significance at p < 0.01; one-way ANOVA.

MiR-199a-3p directly targeted the 3′ UTR of TAOK1 and β-TrCP, the latter acting as the E3 ubiquitin ligase driving YAP degradation through the proteasome (Zhao et al., 2010). Of interest, individual downregulation of either TAOK1 or β-TrCP by RNAi was sufficient to stimulate CM proliferation, indicating that the effect of miR-199a is likely the combinatorial outcome of the downregulation of these (and other) genes impacting on the same pathway. Given that TAOK1 and, in particular, β-TrCP (Fuchs et al., 2004) are involved in several cellular processes, it might well be envisaged that miR-199a might also exert additional functions in CMs in addition to stimulating their replication.

Besides the Hippo pathway, another molecular signature common for several of the investigated miRNAs was the modulation of the actin cytoskeleton network. In particular, we observed a shift in the balance between F- and G-actin toward the polymerized state for all the miRNAs, in particular for miR-199a-3p, miR-302d, miR-373, and miR-33b*. Consistent with this effect, cells treated with miR-199a-3p or miR-373 microscopically showed a rounded morphology and displayed formation of layers of cortical, polymerized actin in bundles close to the cytoplasm periphery.

An actin-regulatory protein that was downregulated by treatment with all the miRNAs, with the exception of miR-590-3p, was Cofilin2. This protein is a muscle-specific member of the ADF/Cofilins family of proteins, which is essential to modulate actin filament non-equilibrium assembly and disassembly, and is thus involved in all aspects of cell motility, locomotion, and invasion (Bernstein and Bamburg, 2010; Bravo-Cordero et al., 2013). In particular, Cofilin binds actin monomers and filaments, causing depolymerization of actin filaments and preventing their reassembly (Ghosh et al., 2004). Of note, four of the miRNAs that we investigated (miR-199a-3p, miR-1825, miR-302d, and miR-373) directly targeted the Cofilin2 3′ UTR. Even more notably, the downregulation of Cofilin2 itself by a specific siRNA was sufficient to stimulate CM proliferation and to activate YAP

nuclear translocation and transactivation of YAP-target genes, while inhibition of actin polymerization by cytochalasin D (a potent inhibitor of actin polymerization) blocked this effect. These results are consistent with previous findings in other cell types showing that the actin cytoskeleton dynamics is a strong activator signal for YAP in response to mechanical cues ensuing from the extracellular environment (Dupont et al., 2011).

The interplay between YAP activation and the cytoskeletal arrangement of CMs has an additional layer of complexity, because recent work has shown that YAP directly regulates genes encoding for proteins that promote F-actin polymerization and link the actin cytoskeleton to the extracellular environment, including components of the dystrophin glycoprotein complex (Morikawa et al., 2015). A component of this complex, Dag1, directly binds YAP and inhibits its pro-proliferative function (Morikawa et al., 2017). Because the dystrophin glycoprotein complex connects the extracellular matrix to the actin cytoskeleton, it is conceivable that perturbing integrity of this connection at different levels might lead to YAP activation.

The discovery that individual miRNAs regulate post-natal CM proliferation is of particular interest toward the potential utilization of these molecules to promote cardiac regeneration. The identification of the molecular targets of the pro-proliferative miRNA is particularly important in this context. The results presented here indicate that stimulation of CM proliferation by miRNAs is a process that requires multiple targeting with likely additive effect. In this respect, the pleiotropic effect of miRNAs appears to be of significant advantage compared to the use of single genes or siRNA knockdowns, provided that the potential deleterious effects are minimized. For example, miR-199a-3p, one of the most effective miRNAs both *ex vivo* and *in vivo*, targets directly the 3′ UTRs of Cofilin2 (modulation of actin cytoskeleton), TAOK1 (activation of the YAP inhibitory kinases), and β-TrCP (reduction of YAP degradation), in addition to the 3′ UTRs of Hopx1 (a suppressor of embryonic CM proliferation) (Trivedi et al., 2010) and Homer1 (involved in the regulation of calcium signaling in cardiac cells) (Jardin et al., 2013), as shown in our previous work (Eulalio et al., 2012). Additional mRNAs could be targeted as well.

Despite this pleiotropic gene downregulation, however, it is of note that all the pro-proliferative pathways appear to converge and require YAP activation. This conclusion is consistent with our previous observation, unexplained at the time, that combinatorial combinations of the four most effective miRNAs in our original HTS screen did not exert an effect that was superior to that of each individual miRNA when used at the same concentration of the combined molecules (Eulalio et al., 2012).

While the pleiotropic function of miRNAs appears highly desirable to stimulate a complex biological event such as differentiated CM proliferation, these molecules need to be considered with caution in translational terms. While the permanent expression of miR-199a and miR-590 pri-miRNAs using AAV9 vectors in the mouse did not result in apparent deleterious effects (Eulalio et al., 2012), permanent expression of the miR-302/367 cluster led transgenic animals to develop cardiac dysfunction due to CM hyperproliferation coupled with cell de-differentiation (Tian et al., 2015). This is consistent with the observation that miR-302/367 enhances the reprogramming efficiency of mouse embryonic fibroblasts into induced pluripotent stem cells (iPSCs) (Judson et al., 2009; Li et al., 2011). In addition, recent work from our laboratory has shown that cardiac delivery of miR-199a after myocardial infarction in pigs using a viral vector driving its persistent expression stimulates cardiac regeneration in the first month after treatment; however, it causes sudden arrhythmic deaths in several of the treated animals at longer observation (Gabisonia et al., 2019). Thus, the permanent expression of these molecules does not appear desirable because of the unwanted effects they may cause.

This note of caution, however, does not rule out that appropriate dose and schedule for the delivery of synthetic miRNA mimics, in contrast to permanent expression, would be effective and well tolerated. Available evidence already shows that single dose, systemic injection of miR302b/c (Tian et al., 2015) or intracardiac injection of miR-199a-3p mimics (Lesizza et al., 2017) determine significant beneficial effects in terms of recovery of myocardial tissue and function in mice. These observations warrant further translation of synthetic pro-regenerative miRNAs to large animals first and to the clinics later.

STAR★METHODS

Detailed methods are provided in the online version of this paper and include the following:

- KEY RESOURCES TABLE
- CONTACT FOR REAGENT AND RESOURCE SHARING
- EXPERIMENTAL MODEL AND SUBJECT DETAILS
  - Animal studies
  - Isolation of ventricular cardiomyocytes
- METHOD DETAILS
  - miRNA/siRNA transfection and EdU incorporation
  - Immunofluorescence
  - TEAD reporter assay
  - Luciferase 3′-UTR reporter assays
  - Nuclear/cytoplasmic fractionation
  - Cardiomyocyte treatments
  - G/F actin separation and immunoblotting
  - ATPlite luminescence assay
  - RNA isolation and quantitative real-time PCR
- QUANTIFICATION AND STATISTICAL ANALYSIS
  - Statistical analysis
  - Bioinformatics
  - Clustering of fold change expression levels
  - Bioinformatic target prediction
- DATA AND SOFTWARE AVAILABILITY

SUPPLEMENTAL INFORMATION

Supplemental Information can be found online at https://doi.org/10.1016/j.celrep.2019.05.005.

ACKNOWLEDGMENTS

The authors are grateful to Willy De Mattia and Stefano Artico for the efficient assistance for animal experimentation. This work was supported by European Research Council (ERC) (250124 to M.G.), Leducq Foundation Transatlantic Network of Excellence (14CVD04 to M.G.), the University of Trieste

(FRA2018 to C.C.), and the Fondazione CRTrieste, Trieste, Italy. C.T., L.B., H.A., and G.P. were supported by ICGEB Arturo Falaschi pre- and post-doctoral fellowships. E.D. was supported by an EMBO long-term fellowship (EMBO ALTF 848-2013) and a FP7 Marie Curie Intra-European Fellowship (project number 627539).

AUTHOR CONTRIBUTIONS

C.T., E.D., L.B., H.A., G.P., M.I.G., and C.C. performed molecular and immunofluorescence analysis. R.J.C., D.L., M.V., M. Marsili, and A.S. performed bioinformatics analysis. L.Z., M. Mano, and S.Z. provided essential advice for the experimental design and assisted in writing the manuscript. M.G. supervised the project and wrote the manuscript.

DECLARATION OF INTERESTS

The authors declare no competing financial interests. The use of some of the microRNAs described in work for cardiac regeneration is covered by patent "MicroRNAs for cardiac regeneration through induction of cardiac myocyte proliferation," grant 2794882.

Received: July 20, 2017
Revised: May 3, 2018
Accepted: April 30, 2019
Published: May 28, 2019

REFERENCES

Agarwal, V., Bell, G.W., Nam, J.W., and Bartel, D.P. (2015). Predicting effective microRNA target sites in mammalian mRNAs. eLife *4*, Published online August 12, 2015. https://doi.org/10.7554/eLife.05005.

Barroso-del Jesus, A., Lucena-Aguilar, G., and Menendez, P. (2009). The miR-302-367 cluster as a potential stemness regulator in ESCs. Cell Cycle *8*, 394–398.

Bernstein, B.W., and Bamburg, J.R. (2010). ADF/cofilin: a functional node in cell biology. Trends Cell Biol. *20*, 187–195.

Bettencourt-Dias, M., Mittnacht, S., and Brockes, J.P. (2003). Heterogeneous proliferative potential in regenerative adult newt cardiomyocytes. J. Cell Sci. *116*, 4001–4009.

Boggiano, J.C., Vanderzalm, P.J., and Fehon, R.G. (2011). Tao-1 phosphorylates Hippo/MST kinases to regulate the Hippo-Salvador-Warts tumor suppressor pathway. Dev. Cell *21*, 888–895.

Bravo-Cordero, J.J., Magalhaes, M.A., Eddy, R.J., Hodgson, L., and Condeelis, J. (2013). Functions of cofilin in cell locomotion and invasion. Nat. Rev. Mol. Cell Biol. *14*, 405–415.

Canseco, D.C., Kimura, W., Garg, S., Mukherjee, S., Bhattacharya, S., Abdisalaam, S., Das, S., Asaithamby, A., Mammen, P.P., and Sadek, H.A. (2015). Human ventricular unloading induces cardiomyocyte proliferation. J. Am. Coll. Cardiol. *65*, 892–900.

Chen, J., Huang, Z.P., Seok, H.Y., Ding, J., Kataoka, M., Zhang, Z., Hu, X., Wang, G., Lin, Z., Wang, S., et al. (2013). mir-17-92 cluster is required for and sufficient to induce cardiomyocyte proliferation in postnatal and adult hearts. Circ. Res. *112*, 1557–1566.

Collesi, C., Zentilin, L., Sinagra, G., and Giacca, M. (2008). Notch1 signaling stimulates proliferation of immature cardiomyocytes. J. Cell Biol. *183*, 117–128.

Del Re, D.P., Yang, Y., Nakano, N., Cho, J., Zhai, P., Yamamoto, T., Zhang, N., Yabuta, N., Nojima, H., Pan, D., and Sadoshima, J. (2013). Yes-associated protein isoform 1 (Yap1) promotes cardiomyocyte survival and growth to protect against myocardial ischemic injury. J. Biol. Chem. *288*, 3977–3988.

Diez-Cuñado, M., Wei, K., Bushway, P.J., Maurya, M.R., Perera, R., Subramaniam, S., Ruiz-Lozano, P., and Mercola, M. (2018). miRNAs that Induce Human Cardiomyocyte Proliferation Converge on the Hippo Pathway. Cell Rep. *23*, 2168–2174.

Dobin, A., Davis, C.A., Schlesinger, F., Drenkow, J., Zaleski, C., Jha, S., Batut, P., Chaisson, M., and Gingeras, T.R. (2013). STAR: ultrafast universal RNA-seq aligner. Bioinformatics *29*, 15–21.

Dupont, S., Morsut, L., Aragona, M., Enzo, E., Giulitti, S., Cordenonsi, M., Zanconato, F., Le Digabel, J., Forcato, M., Bicciato, S., et al. (2011). Role of YAP/TAZ in mechanotransduction. Nature *474*, 179–183.

Engel, F.B., Schebesta, M., Duong, M.T., Lu, G., Ren, S., Madwed, J.B., Jiang, H., Wang, Y., and Keating, M.T. (2005). p38 MAP kinase inhibition enables proliferation of adult mammalian cardiomyocytes. Genes Dev. *19*, 1175–1187.

Eschenhagen, T., Bolli, R., Braun, T., Field, L.J., Fleischmann, B.K., Frisén, J., Giacca, M., Hare, J.M., Houser, S., Lee, R.T., et al. (2017). Cardiomyocyte Regeneration: A Consensus Statement. Circulation *136*, 680–686.

Eulalio, A., Mano, M., Dal Ferro, M., Zentilin, L., Sinagra, G., Zacchigna, S., and Giacca, M. (2012). Functional screening identifies miRNAs inducing cardiac regeneration. Nature *492*, 376–381.

Frémont, S., Romet-Lemonne, G., Houdusse, A., and Echard, A. (2017). Emerging roles of MICAL family proteins - from actin oxidation to membrane trafficking during cytokinesis. J. Cell Sci. *130*, 1509–1517.

Fuchs, S.Y., Spiegelman, V.S., and Kumar, K.G. (2004). The many faces of beta-TrCP E3 ubiquitin ligases: reflections in the magic mirror of cancer. Oncogene *23*, 2028–2036.

Gabisonia, K., Prosdocimo, G., Aquaro, G.D., Carlucci, L., Zentilin, L., Secco, I., Ali, A., Braga, L., Gorgodze, N., Bernini, F., et al. (2019). MicroRNA therapy stimulates uncontrolled cardiac repair after myocardial infarction in pigs. Nature, Published online May 8, 2019. https://doi.org/10.1038/s41586-019-1191-6.

Ghosh, M., Song, X., Mouneimne, G., Sidani, M., Lawrence, D.S., and Condeelis, J.S. (2004). Cofilin promotes actin polymerization and defines the direction of cell motility. Science *304*, 743–746.

Giacca, M., and Zacchigna, S. (2015). Harnessing the microRNA pathway for cardiac regeneration. J. Mol. Cell. Cardiol. *89* (*Pt A*), 68–74.

Heallen, T., Zhang, M., Wang, J., Bonilla-Claudio, M., Klysik, E., Johnson, R.L., and Martin, J.F. (2011). Hippo pathway inhibits Wnt signaling to restrain cardiomyocyte proliferation and heart size. Science *332*, 458–461.

Heallen, T., Morikawa, Y., Leach, J., Tao, G., Willerson, J.T., Johnson, R.L., and Martin, J.F. (2013). Hippo signaling impedes adult heart regeneration. Development *140*, 4683–4690.

Huang, W., Sherman, B.T., and Lempicki, R.A. (2009a). Bioinformatics enrichment tools: paths toward the comprehensive functional analysis of large gene lists. Nucleic Acids Res. *37*, 1–13.

Huang, W., Sherman, B.T., and Lempicki, R.A. (2009b). Systematic and integrative analysis of large gene lists using DAVID bioinformatics resources. Nat. Protoc. *4*, 44–57.

Jardin, I., López, J.J., Berna-Erro, A., Salido, G.M., and Rosado, J.A. (2013). Homer proteins in Ca^{2+} entry. IUBMB Life *65*, 497–504.

Judson, R.L., Babiarz, J.E., Venere, M., and Blelloch, R. (2009). Embryonic stem cell-specific microRNAs promote induced pluripotency. Nat. Biotechnol. *27*, 459–461.

Laflamme, M.A., and Murry, C.E. (2011). Heart regeneration. Nature *473*, 326–335.

Lesizza, P., Prosdocimo, G., Martinelli, V., Sinagra, G., Zacchigna, S., and Giacca, M. (2017). Single-Dose Intracardiac Injection of Pro-Regenerative MicroRNAs Improves Cardiac Function After Myocardial Infarction. Circ. Res. *120*, 1298–1304.

Li, Z., Yang, C.S., Nakashima, K., and Rana, T.M. (2011). Small RNA-mediated regulation of iPS cell generation. EMBO J. *30*, 823–834.

Martin, M. (2011). Cutadapt removes adapter sequences from high-throughput sequencing reads. EMBnetjournal *17*, 10–12.

Matsui, Y., Nakano, N., Shao, D., Gao, S., Luo, W., Hong, C., Zhai, P., Holle, E., Yu, X., Yabuta, N., et al. (2008). Lats2 is a negative regulator of myocyte size in the heart. Circ. Res. *103*, 1309–1318.

McCarthy, D.J., Chen, Y., and Smyth, G.K. (2012). Differential expression analysis of multifactor RNA-Seq experiments with respect to biological variation. Nucleic Acids Res. *40*, 4288–4297.

Morikawa, Y., Zhang, M., Heallen, T., Leach, J., Tao, G., Xiao, Y., Bai, Y., Li, W., Willerson, J.T., and Martin, J.F. (2015). Actin cytoskeletal remodeling with protrusion formation is essential for heart regeneration in Hippo-deficient mice. Sci. Signal. *8*, ra41.

Morikawa, Y., Heallen, T., Leach, J., Xiao, Y., and Martin, J.F. (2017). Dystrophin-glycoprotein complex sequesters Yap to inhibit cardiomyocyte proliferation. Nature *547*, 227–231.

Nakada, Y., Canseco, D.C., Thet, S., Abdisalaam, S., Asaithamby, A., Santos, C.X., Shah, A.M., Zhang, H., Faber, J.E., Kinter, M.T., et al. (2017). Hypoxia induces heart regeneration in adult mice. Nature *541*, 222–227.

NCBI Resource Coordinators (2017). Database Resources of the National Center for Biotechnology Information. Nucleic Acids Res. *45* (*D1*), D12–D17.

Pan, D. (2010). The hippo signaling pathway in development and cancer. Dev. Cell *19*, 491–505.

Papalouka, V., Arvanitis, D.A., Vafiadaki, E., Mavroidis, M., Papadodima, S.A., Spiliopoulou, C.A., Kremastinos, D.T., Kranias, E.G., and Sanoudou, D. (2009). Muscle LIM protein interacts with cofilin 2 and regulates F-actin dynamics in cardiac and skeletal muscle. Mol. Cell. Biol. *29*, 6046–6058.

Plouffe, S.W., Meng, Z., Lin, K.C., Lin, B., Hong, A.W., Chun, J.V., and Guan, K.L. (2016). Characterization of Hippo Pathway Components by Gene Inactivation. Mol. Cell *64*, 993–1008.

Poon, C.L., Lin, J.I., Zhang, X., and Harvey, K.F. (2011). The sterile 20-like kinase Tao-1 controls tissue growth by regulating the Salvador-Warts-Hippo pathway. Dev. Cell *21*, 896–906.

Porrello, E.R., Mahmoud, A.I., Simpson, E., Hill, J.A., Richardson, J.A., Olson, E.N., and Sadek, H.A. (2011). Transient regenerative potential of the neonatal mouse heart. Science *331*, 1078–1080.

Poss, K.D., Wilson, L.G., and Keating, M.T. (2002). Heart regeneration in zebrafish. Science *298*, 2188–2190.

Ritchey, L., and Chakrabarti, R. (2014). Aurora A kinase modulates actin cytoskeleton through phosphorylation of Cofilin: Implication in the mitotic process. Biochim. Biophys. Acta *1843*, 2719–2729.

Saucedo, L.J., and Edgar, B.A. (2007). Filling out the Hippo pathway. Nat. Rev. Mol. Cell Biol. *8*, 613–621.

Tian, Y., Liu, Y., Wang, T., Zhou, N., Kong, J., Chen, L., Snitow, M., Morley, M., Li, D., Petrenko, N., et al. (2015). A microRNA-Hippo pathway that promotes cardiomyocyte proliferation and cardiac regeneration in mice. Sci. Transl. Med. *7*, 279ra38.

Tiscornia, G., and Izpisúa Belmonte, J.C. (2010). MicroRNAs in embryonic stem cell function and fate. Genes Dev. *24*, 2732–2741.

Trivedi, C.M., Zhu, W., Wang, Q., Jia, C., Kee, H.J., Li, L., Hannenhalli, S., and Epstein, J.A. (2010). Hopx and Hdac2 interact to modulate Gata4 acetylation and embryonic cardiac myocyte proliferation. Dev. Cell *19*, 450–459.

van Rooij, E. (2011). The art of microRNA research. Circ. Res. *108*, 219–234.

von Gise, A., Lin, Z., Schlegelmilch, K., Honor, L.B., Pan, G.M., Buck, J.N., Ma, Q., Ishiwata, T., Zhou, B., Camargo, F.D., and Pu, W.T. (2012). YAP1, the nuclear target of Hippo signaling, stimulates heart growth through cardiomyocyte proliferation but not hypertrophy. Proc. Natl. Acad. Sci. USA *109*, 2394–2399.

Wang, J., Fan, Y., Dube, D.K., Sanger, J.M., and Sanger, J.W. (2014a). Jasplakinolide reduces actin and tropomyosin dynamics during myofibrillogenesis. Cytoskeleton (Hoboken) *71*, 513–529.

Wang, P., Mao, B., Luo, W., Wei, B., Jiang, W., Liu, D., Song, L., Ji, G., Yang, Z., Lai, Y.Q., and Yuan, Z. (2014b). The alteration of Hippo/YAP signaling in the development of hypertrophic cardiomyopathy. Basic Res. Cardiol. *109*, 435.

Xin, M., Kim, Y., Sutherland, L.B., Qi, X., McAnally, J., Schwartz, R.J., Richardson, J.A., Bassel-Duby, R., and Olson, E.N. (2011). Regulation of insulin-like growth factor signaling by Yap governs cardiomyocyte proliferation and embryonic heart size. Sci. Signal. *4*, ra70.

Xin, M., Kim, Y., Sutherland, L.B., Murakami, M., Qi, X., McAnally, J., Porrello, E.R., Mahmoud, A.I., Tan, W., Shelton, J.M., et al. (2013a). Hippo pathway effector Yap promotes cardiac regeneration. Proc. Natl. Acad. Sci. USA *110*, 13839–13844.

Xin, M., Olson, E.N., and Bassel-Duby, R. (2013b). Mending broken hearts: cardiac development as a basis for adult heart regeneration and repair. Nat. Rev. Mol. Cell Biol. *14*, 529–541.

Xue, B., and Robinson, R.C. (2013). Guardians of the actin monomer. Eur. J. Cell Biol. *92*, 316–332.

Yamamoto, S., Yang, G., Zablocki, D., Liu, J., Hong, C., Kim, S.J., Soler, S., Odashima, M., Thaisz, J., Yehia, G., et al. (2003). Activation of Mst1 causes dilated cardiomyopathy by stimulating apoptosis without compensatory ventricular myocyte hypertrophy. J. Clin. Invest. *111*, 1463–1474.

Zacchigna, S., and Giacca, M. (2014). Extra- and intracellular factors regulating cardiomyocyte proliferation in postnatal life. Cardiovasc. Res. *102*, 312–320.

Zhao, B., Ye, X., Yu, J., Li, L., Li, W., Li, S., Yu, J., Lin, J.D., Wang, C.Y., Chinnaiyan, A.M., et al. (2008). TEAD mediates YAP-dependent gene induction and growth control. Genes Dev. *22*, 1962–1971.

Zhao, B., Li, L., Tumaneng, K., Wang, C.Y., and Guan, K.L. (2010). A coordinated phosphorylation by Lats and CK1 regulates YAP stability through SCF(beta-TRCP). Genes Dev. *24*, 72–85.

STAR★METHODS

KEY RESOURCES TABLE

REAGENT or RESOURCE	SOURCE	IDENTIFIER
Antibodies		
Rabbit polyclonal anti-YAP	Cell Signaling Tecnology	Cat# 4912S RRID:AB_10694682
Rabbit polyclonal anti-Phospho YAP (Ser 127)	Cell Signaling Tecnology	Cat# 4911S RRID:AB_2218913
Rabbit polyclonal anti-Cofilin 2	Millipore	Cat# 07-300 RRID:AB_2080926
Mouse monoclonal anti-F actin	Abcam	Cat# ab205 RRID:AB_302794 Clone NH3
Rabbit polyclonal anti-alpha-actin	Cytoskeleton	Cat# AAN01 also AAN01-B,AAN01-A RRID:AB_10708070
Rabbit polyclonal anti-β-TrCP/HOS	Santa Cruz Biotechnology	Cat# sc-15354 RRID:AB_2065916
Rabbit polyclonal anti-GAPDH	Santa Cruz Biotechnology	Cat# sc-25778 RRID:AB_10167668
Rabbit polyclonal anti-PARP-1	Enzo Life Sciences	Cat# ALX-210-302 RRID:AB_2160732
Mouse monoclonal anti-p84	Abcam	Cat# ab487 RRID:AB_304696 Clone 5E10
Mouse monoclonal anti-Sarcomeric Alpha Actinin	Abcam	Cat# ab9465 RRID:AB_307264
Alexa fluor 488 phalloidin	Thermo Fisher Scientific	Cat# A12379 also A-12379 RRID:AB_2315147
Rabbit polyclonal anti-TAOK1	LifeSpan BioSciences, Inc.	Cat# LS-C146952 Lot# 62983 RRID:AB_11132558
Rabbit polyclonal anti-STK38L/Ndr2	Abcam	Cat# ab126106 RRID:AB_11129556
Chemicals, Peptides, and Recombinant Proteins		
FuGENE HD Transfection Reagent	Promega	Cat#E2312
Cytochalasin D	Santa Cruz	Cat#sc-201442
Oligofectamine	Thermo Scientific	Cat#12252011
RNAiMAX	Thermo Scientific	Cat#13778150
Jasplakinolide	Sigma	Cat#J4580
Bovine FGF acidic Protein	R&D Systems	Cat#132-FA
P38 inhibitor	Calbiochem	Cat#SB203580
Phenylephrine	Sigma	Cat#P6126
Critical Commercial Assays		
G-actin/F-actin *In Vivo* Assay kit	Cytoskeleton, Inc	Cat#BK037
Dual-Glo Luciferase assay System	Promega	Cat#E2940
Click-IT EdU Alexa Fluor 594 Imaging kit	Thermo Scientific	Cat#C10339
CTGF TaqMan Gene Expression Assay	Thermo Scientific	Assay ID Rn01537279_g1
CyR61 TaqMan Gene Expression Assay	Thermo Scientific	Assay ID Rn00580055_m1
TAOK1 TaqMan Gene Expression Assay	Thermo Scientific	Assay ID Rn00597907_m1
β-TrCP TaqMan Gene Expression Assay	Thermo Scientific	Assay ID Rn01413748_m1
Cfl2 TaqMan Gene Expression Assay	Thermo Scientific	Assay ID Rn01472820_g1
STK38L TaqMan Gene Expression Assay	Thermo Scientific	Assay ID Rn01472820_g1
Deposited Data		
mRNA sequence data of neonatal rat cardiomyocytes after transfection of hsa-miR-302d	This Study	Accession GSM3716799
mRNA sequence data of neonatal rat cardiomyocytes after transfection of hsa-miR-373-3p	This Study	Accession GSM3716798
mRNA sequence data of neonatal rat cardiomyocytes after transfection of hsa-miR-33b*	This Study	Accession GSM3716800
mRNA sequence data of neonatal rat cardiomyocytes after transfection of hsa-miR-1825	This Study	Accession GSM3716801
mRNA sequence data of neonatal rat cardiomyocytes after transfection of hsa-miR-199a-3p	This Study	Accession GSM3716796

(*Continued on next page*)

Continued

REAGENT or RESOURCE	SOURCE	IDENTIFIER
mRNA sequence data of neonatal rat cardiomyocytes after transfection of hsa-miR-590-3p	This Study	Accession GSM3716797
mRNA sequence data of neonatal rat cardiomyocytes after transfection of cel-miR-67	This Study	Accession GSM3716795
Experimental Models: Cell Lines		
HeLa cell line	ATCC	Cat# CCL-2, RRID:CVCL_0030
Experimental Models: Organisms/Strains		
Wistar neonatal Rat	Harlan	N/A
Oligonucleotides		
siRNA YAP1 sense: 5′- GGAGAAGUUUACUACAUAA [dT] [dT] −3′	Sigma	siRNA targeting sequence: YAP1 NM_001034002.2
siRNA YAP1 antisense: 5′-UUAUGUAGUAAACUUCUCC [dT] [dT] −3′	Sigma	siRNA targeting sequence: YAP1 NM_001034002.2
siGenome SMARTpool against rat Cfl2	Dharmacon	cat# M-099723-01
siGenome SMARTpool against rat TAOK1	Dharmacon	cat# M-095482-01
siGenome SMARTpool against rat β-TrCP	Dharmacon	cat# M-086092-01
siRNA against rat STK38L	Sigma	ID: SASI Rn02_00208859
MISSION siRNA Universal Negative Control #1	Sigma	Cat#SIC001
siGENOME Non-Targeting siRNA #4	Dharmacon	Cat#D-001210-04
Recombinant DNA		
p8xGTIIC-Luc plasmid	Gift from Stefano Piccolo, University of Padova	Addgene, Cat#34615
pRL Renilla Luciferase control plasmid	Promega	cat# E2261
5SA-YAP1 in pCSII-EF-MCS plasmid	Gift from Stefano Piccolo, University of Padova	N/A
psiCheck2.1 plasmid	Promega	Cat# C8021
3′UTR-Cfl2 plasmid	Biomatik	Clone ID T4545-1
3′UTR-β-TrC plasmid	Genewiz	Clone ID B28633-1/K28633
3′UTR-TAOK1 plasmid	Genewiz	
3′UTR-mut TAOK1 plasmid	QuikChange II XL Site-Directed Mutagenesis Kit	N/A
3′UTR-mut β-TrC plasmid	QuikChange II XL Site-Directed Mutagenesis Kit	N/A
3′UTR-STK38L plasmid	IDT gblock	N/A
3′UTR-Cfl2mut plasmid	IDT gblock	N/A
Software and Algorithms		
Clustering algorithm	https://www.scipy.org	N/A
Functional analysis	https://david.ncifcrf.gov	Huang et al., 2009a, 2009b
FASTQC software	http://www.bioinformatics.babraham.ac.uk/projects/fastqc	N/A
Cutadapt software	N/A	Martin, 2011
STAR software	N/A	Dobin et al., 2013
Bioconductor package edgeR rpkm function	N/A	McCarthy et al., 2012
Rattus Norvegicus reference genome	GCF_000001895.5 Rnor 6.0.82	N/A
TargetScan Software release 7.1	http://www.targetscan.org	N/A
miRBase 21 database	http://www.mirbase.org	N/A

CONTACT FOR REAGENT AND RESOURCE SHARING

Further information and request for resources and reagents should be directed to and will be fulfilled by the Lead Contact, Mauro Giacca (mauro.giacca@kcl.ac.uk).

EXPERIMENTAL MODEL AND SUBJECT DETAILS

Animal studies

Animal care and treatment were conducted in conformity with institutional guidelines after approval by the ICGEB Institutional Review Board following consent from the Italian Ministry of Health in accordance with the Italian law (D.lgs. 26/2014), following European Union policies (European and Economic Council Directive 86/609, OJL 358, December 12, 1987).

Isolation of ventricular cardiomyocytes

Ventricular CMs were isolated from both male and female neonatal rats as previously described (Collesi et al., 2008). Briefly, ventricles from neonatal (P0) rats were separated from the atria, cut into pieces and then dissociated in calcium and bicarbonate-free Hanks with HEPES (CBFHH) buffer containing 1.75 mg/ml trypsin (BD Difco) and 10 mg/ml DNase II (Sigma), using mechanical and physical stirring. Digestion was performed at room temperature in ten 10-min steps with collection of the supernatant to fetal bovine serum (FBS, Life Technologies) after each step. The collected supernatant was centrifuged to pellet the cells, which were then resuspended in Dulbecco's modified Eagle medium 4.5 g/l glucose (DMEM, Life Technologies) supplemented with 5% FBS, 20 mg/ml vitamin B12 (Sigma) and 100 U/ml penicillin and 100 mg/ml streptomycin (Sigma). The collected cells were passed through a cell strainer (40 mm, BD Falcon) and then seeded onto four 100-mm plastic dishes for 2 hr at 37 °C in 5% CO2 and humidified atmosphere. The supernatant, composed mostly of CMs, was then collected, counted and plated at the appropriate density into BD Matrigel Matrix Growth Factor Reduced (356230 BD Bioscience) pre-coated Primaria 96-well plates (BD Falcon) or matrigel-coated Primaria 35-mm dishes (BD Falcon).

METHOD DETAILS

miRNA/siRNA transfection and EdU incorporation

MicroRNAs and siRNAs (SMARTpool) were obtained from Dharmacon, Thermo Scientific and transfected into neonatal rat CMs using a standard reverse transfection protocol (Eulalio et al., 2012). Briefly, a transfection reagent (Lipofectamine RNAiMAX, Life Technologies) was diluted in OPTI-MEM (Life Technologies) and added to the miRNAs, siRNAs or a combination of the two (at a final concentration of 25 nM each nucleic acid), arrayed on 96-well plates; 30 min later, $1x10^4$ cells were seeded per well. Twenty-four hr after transfection, the culture medium was replaced by fresh medium; 28 h later, that is, 52 h after plating, the culture medium was replaced with medium containing 5 mM 5- ethynyl-29-deoxyuridine (EdU, Life Technologies) for 20 h. Cells were fixed at 72 h after plating and processed for immunofluorescence. Experiments were performed in quadruplicate.

Immunofluorescence

CMs were fixed with 4% PFA for 10 min, permeabilized with 0.5% Triton X-100 in PBS for 10 min, followed by 1 hr blocking in 2% BSA (Roche). CMs were then stained overnight at 4 °C with mouse monoclonal antibody against sarcomeric α-actinin (Abcam) diluted in blocking solution. Cells were washed with PBS and incubated for 2 hr with the secondary antibody conjugated to Alexa Fluor-488 (Life Technologies). Cells were further processed using the Click-IT EdU 555 Imaging kit (Life Technologies) to reveal EdU incorporation, according to the manufacturer's instructions, and stained with Hoechst 33342.

TEAD reporter assay

For luciferase assays, CMs were plated at the concentration of $1.5x10^5$ (day 0) in a double-matrigel coated 96-Multiwell plate and, the subsequent day, were transfected with the selected miRNAs (Dharmacon). At day 2, the culture medium was replaced. At day 3, cells were transfected with 100 ng of both synthetic TEAD reporter firefly luciferase plasmid (p8xGTIIC-Lux, Plasmid #34615, Addgene) and a Renilla luciferase plasmid in OPTI-MEM (Life Technologies). After 4 hr, the medium was replaced with DMEM, Life Technologies, supplemented with 5% FBS, 20 mg/ml vitamin B12 (Sigma) and with 100 U/ml of penicillin and 100 mg/ml of streptomycin (Sigma). After 24 hr, firefly and fenilla luciferase activities were measured using the Dual Luciferase Reporter Assay System (Promega), according to the manufacturer's instructions.

Luciferase 3′-UTR reporter assays

Constructs bearing the rat 3′-UTR of Cofilin2, TAOK1 and β-TrCP were obtained by gene synthesis from Biomatik (3′UTR-Cfl2), Genewiz (3′UTR- β-TrCP and 3′UTR-TAOK1) or Integrated DNA Technology (3′ UTR-STK38L; gBlocks DNA synthesis) and subcloned into psiCHECK2.1 vector (Promega). HeLa cells were transfected with the miRNA under investigation at a final concentration of 50 nM in 96-well plates, through a standard reverse transfection protocol similar to that described above. Twenty-four hr later, cells were transfected with 100 ng per well of the reporter constructs or psiCHECK2 vector (control) using FuGENE HD transfection reagent (Promega). Firefly and Renilla luciferase activities were measured 48 hr after plasmid transfection using the Dual Luciferase Reporter Assay System (Promega), according to the manufacturer's instructions. The mutated 3′-UTR of β-TrC and TAOK1 were obtained by using QuikChange II XL Site-Directed Mutagenesis Kit according to the manufacturer's instructions using overlapping primers bearing the mutated sequences reported in Figure S3. The mutated 3′-UTR of Cofilin2 was obtained by gene synthesis

(gBlocks) from Integrated DNA Technology. In all cases, the mutated sequences were cloned into the psiCHECK2.1 vector. The DNA sequence of all constructs was verified by Sanger sequencing.

Nuclear/cytoplasmic fractionation

Cells ($1x10^6$ cells were plated in matrigel-coated Primaria 60-mm dishes (BD Falcon) as described above. miRNAs were transfected by a standard forward transfection protocol. Seventy-two hr after transfection, cells were washed with ice-cold PBS and harvested in 80 μl of hypotonic buffer (50 mM Tris pH7.5, 10 mM NaCl, 3 mM $MgCl_2$, 10% glycerol) supplemented with protease inhibitors (complete tablets, Mini EDTA-free, Roche) and phosphatase inhibitors (cocktail 3 Sigma, 2mM orthovanadate, 1 mM NaF). After 1 min, cells were scraped and NP40 was added at 0.1% final concentration. After 5 min on ice, cells were centrifuged at 4000 rpm for 5 min at 4°C; the supernatant and cytosolic fractions were then recovered. Pellets were resuspended in 70 μl IPLS buffer (50 mM Tris pH 7.5, 120 mM NaCl, 1 mM EDTA, 0.5% NP40, supplemented with the same inhibitors as above) and sonicated with 3 pulses of 10 min each (30 s on/30sec off) on ice in a Bioruptor Plus (Biosense). Nuclear lysates were centrifuged at 16,000 rpm for 20 min at 4°C and the supernatant was recovered as nuclear fraction. Concentration of cytoplasmic and nuclear lysates were measured using the Bradford assay (Protein Assay Dye Reagent Concentrate, Bio Rad). Lysates (10 to 20 μg) were loaded for protein separation and subsequent blotting onto a PVDF membrane (Amersham Hybond PVDF, GE Healthcare).

Cardiomyocyte treatments

Cytochalasin D (sc_201442, Santa Cruz) was added to the CM culture medium at the final concentration of 0.1 μM for 2-6 hr; Jasplakinolide (J4580, Sigma-Aldrich) at 0.5 μM for 30-90 min; FGF1 at 50 ng/mL, readministered every 24 hr for 72 hr; the p38 inhibitor SB203580 at 40 μM for 72 hr; phenylephrine at 50 μM for 24 hr.

G/F actin separation and immunoblotting

The amount of G-actin and F-actin in CMs was quantified using G-actin/F-actin *in vivo* assay kit (Cytoskeleton Inc.) according to the manufacturer's instructions. Briefly, cells were lysed in pre-warmed lysis/F-actin stabilizing buffer supplemented with protease inhibitor and ATP. The cell lysate was centrifuged for 5 min at 350 × g to remove debris. A 100 μl aliquot was then ultracentrifuged at 100,000 × g for 1 hr at 37°C to pellet F-actin, with G-actin remaining in the supernatant. The pellet was resuspended in 100 μl of F-actin destabilizing buffer on ice for 1 hr with frequent pipetting. Equal volumes of G-actin and F-actin fractions were mixed with 5 × SDS sample buffer and run on SDS-PAGE. Western blot analysis was performed using the anti α-actin antibody provided in the kit. Densitometry analysis was performed using the ImageJ software.

ATPlite luminescence assay

ATPlite Luminescence Assay System (PerkinElmer) was performed according to the manufacturer's protocol. Briefly, 50 μL of mammalian cell lysis solution were added to 100 μL CM suspension per well and plates were shaken at 700 rpm for 5 min. Next, 50 μL substrate solution were added to each well, followed by a second round of shaking (5 min at 700 rpm). Luminescence was the measured using a Wallac EnVision™ 2104 MultiLabel Reader.

RNA isolation and quantitative real-time PCR

Total mRNA was isolated from CMs 72 hr after transfection, or at different time points after cytochalasin D treatment, using a standard TRIZOL RNA isolation protocol. The RNA obtained (1 μg) was reverse-transcribed using MLV-RT (Invitrogen) with random hexamers (10 μM) in a 20 μL reaction, following the manufacturer's instructions. mRNA levels for CTGF, CyR61 and GAPDH were measured by Real-Time PCR using pre-designed TaqMan assays (Thermofisher) and iQSupermix (Bio-Rad) according to the manufacturer's instruction.

QUANTIFICATION AND STATISTICAL ANALYSIS

Statistical analysis

Unless otherwise indicated, all data are expressed as mean ± standard error of the mean (SEM). One-way ANOVA followed by post hoc analysis with the Bonferroni's Multiple Comparison Test was used for the analysis of multiple groups; two-tail Student's t test was used to compare two individual groups. GraphPad Prism version 6 was used for statistical analyzes included in the main and supplementary figures of the study.

Bioinformatics

Transcriptomic analysis

Deep-sequencing of total neonatal rat CM RNA was performed 72 hr after transfection of the microRNAs by IGA Technology Services, Udine, Italy as in Eulalio et al. (2012). Briefly, RNA purity, integrity and concentration were determined using an Agilent 2100 Bioanalyzer (Agilent Technologies). Only RNA with a RIN value > 7 and an rRNA 28S/18S ratio > 2 was taken forward for sample preparation. Two μg of total RNA (minimum concentration of 200 ng/μl) per sample were sequenced on an Illumina HiSeq2000. Two lanes in 7-plex were run obtaining 20 million single-reads per sample, 50-bp long. The raw sequencing data discussed in

this publication have been deposited in NCBI's Sequence Read Archive (SRA) and are accessible through SRA STUDY accession SUB2866022.

Real-time image analysis, base calling, de-multiplexing and production of FASTQ sequence files were performed on the HiSeq2000 instrument using the HiSeq Software. Raw sequence files were quality checked using FASTQC software (http://www.bioinformatics.babraham.ac.uk/projects/fastqc) and trimmed to remove Illumina adaptor using Cutadapt software (Martin, 2011). RNA-seq reads were mapped to Rattus norvegicus reference genome (GCF_000001895.5 Rnor 6.0.82) and to known mature miRNAs using STAR software (Dobin et al., 2013). Rounded Gene counts were used as input and transformed to RPKM (reads per kilobase of exon model per million mapped reads) using Bioconductor package edgeR rpkm function (McCarthy et al., 2012).

In the case of transfection of a pro-proliferative miRNA, genes whose RPKM values were greater than 1.00 in both miRNA and cel-miR-67 control-transfected rat CMs were considered as expressed. Fold changes were taken with respect to the expression of cel-miR-67 control. Genes whose fold changes were greater than 1.3 (both upregulated and downregulated) were considered as differentially expressed.

Clustering of fold change expression levels

Cluster analysis was performed on the basis of the log2-fold changes in gene expression in respect to cel-miR-67 to classify the pro-proliferating miRNAs according to their effects on CMs upon transfection. In brief, the correlation between the log2-fold changes for all pairs of miRNAs were calculated. Clusters were then identified hierarchically using the average linkage criterion with a Euclidean distance metric as implemented in the clustering package of SciPy v0.18.1 (https://www.scipy.org). Dendrograms were then generated to visualize the arrangement of the resulting cluster.

Bioinformatic target prediction

To the best of our knowledge, bioinformatic predictions of seed sequence interactions with rat transcripts are not available. Because of this constraint, we compiled a list of rat miRNA-gene interactions from mouse predictions. In particular, predicted mouse gene targets of the seed sequences (corresponding to miRNA families) of pro-proliferative miRNAs were collected from TargetScanMouse Release 7.1 (Agarwal et al., 2015). The mouse genes were then converted to their corresponding rat genes via homology using the HomoloGene database (NCBI Resource Coordinators, 2017). The list of miRNA-gene interactions was filtered to only include genes that were downregulated by the miRNA upon transfection to CMs according to the transcriptomic data.

DATA AND SOFTWARE AVAILABILITY

RNA-seq data have been deposited at GEO under accession GEO: GSE129598.